ARTICLE

Mutations in *OTOGL*, Encoding the Inner Ear Protein Otogelin-like, Cause Moderate Sensorineural Hearing Loss

Kemal O. Yariz,[1,2,15] Duygu Duman,[4,15] Celia Zazo Seco,[5,6,7] Julia Dallman,[9] Mingqian Huang,[10] Theo A. Peters,[5,6,7] Asli Sirmaci,[1,2] Na Lu,[10,11] Margit Schraders,[5,6,7] Isaac Skromne,[9] Jaap Oostrik,[5,6,7] Oscar Diaz-Horta,[1,2] Juan I. Young,[1,2] Suna Tokgoz-Yilmaz,[4] Ozlem Konukseven,[12] Hashem Shahin,[13] Lisette Hetterschijt,[7,8] Moien Kanaan,[13] Anne M.M. Oonk,[5,6] Yvonne J.K. Edwards,[1,2] Huawei Li,[11] Semra Atalay,[4] Susan Blanton,[1,2] Alexandra A. DeSmidt,[9] Xue-Zhong Liu,[1,3,14] Ronald J.E. Pennings,[5,6] Zhongmin Lu,[9] Zheng-Yi Chen,[10] Hannie Kremer,[5,6,7,8] and Mustafa Tekin[1,2,4,*]

Hereditary hearing loss is characterized by a high degree of genetic heterogeneity. Here we present *OTOGL* mutations, a homozygous one base pair deletion (c.1430 delT) causing a frameshift (p.Val477Glufs*25) in a large consanguineous family and two compound heterozygous mutations, c.547C>T (p.Arg183*) and c.5238+5G>A, in a nonconsanguineous family with moderate nonsyndromic sensorineural hearing loss. *OTOGL* maps to the DFNB84 locus at 12q21.31 and encodes otogelin-like, which has structural similarities to the epithelial-secreted mucin protein family. We demonstrate that *Otogl* is expressed in the inner ear of vertebrates with a transcription level that is high in embryonic, lower in neonatal, and much lower in adult stages. Otogelin-like is localized to the acellular membranes of the cochlea and the vestibular system and to a variety of inner ear cells located underneath these membranes. Knocking down of *otogl* with morpholinos in zebrafish leads to sensorineural hearing loss and anatomical changes in the inner ear, supporting that otogelin-like is essential for normal inner ear function. We propose that *OTOGL* mutations affect the production and/or function of acellular structures of the inner ear, which ultimately leads to sensorineural hearing loss.

Introduction

Hereditary hearing loss is characterized by genetic heterogeneity with mutations in several hundreds of genes encoding a variety of proteins.[1–3] Mutations in these genes lead to various clinical scenarios ranging from nonsyndromic hearing loss to one of the more than 400 syndromes that include hearing loss and from mild adult onset hearing loss to profound congenital deafness spanning a full spectrum of Mendelian inheritance.[1,2] The autosomal recessive pattern of inheritance occurs in the majority of families with autosomal recessive nonsyndromic hearing loss (arNSHL) and is typically congenital or prelingual-onset.[2] Mutations in 40 genes have thus far been shown to cause arNSHL, which can account for more than 60% of families with this type of inheritance pattern.[3] Hearing loss is usually severe or profound in cases with arNSHL, although varying degrees of residual hearing are observed in some families. Individuals with mutations in *STRC* (MIM 606440), for example, essentially present with moderate hearing loss[4] and 22% of the persons with mutations in the DFNB1 locus have moderate deafness.[5]

In this study, we report mutations in *OTOGL*, encoding otogelin-like, that are associated with moderate arNSHL. We demonstrate that *OTOGL* is expressed in the inner ears of humans, mouse, rat, and zebrafish, and its disruption in zebrafish leads to hearing loss.

Materials and Methods

Studied Families

The study on hereditary deafness was approved by the Ethics Committees of Ankara University (Turkey) and the Radboud University Nijmegen Medical Centre (The Netherlands), and by the IRB at the University of Miami (USA). Informed consents were obtained from all participants, or in the case of minors, from the parents. Diagnosis of sensorineural hearing loss was established via standard audiometry in a sound-proofed room according to current clinical standards. Hearing loss was classified according to the GENDEAF guidelines (hereditary hearing loss homepage). Evaluation for vestibular function included Unterberger, Romberg, head thrust, and head shake tests, oculomotor examination, spontaneous nystagmus and positioning tests, and bithermal caloric tests via videonystagmography (VNG, Micromedical Technologies, Illinois USA). Slow component velocity (SCV) of the nystagmus was measured with a threshold of

[1]John P. Hussman Institute for Human Genomics, [2]Dr. John T. Macdonald Department of Human Genetics, [3]Department of Otolaryngology , University of Miami Miller School of Medicine, Miami, FL 33136, USA; [4]Division of Pediatric Genetics, Ankara University School of Medicine, 06100 Ankara, Turkey; [5]Department of Otorhinolaryngology, [6]Donders Institute for Brain, Cognition and Behaviour, [7]Nijmegen Centre for Molecular Life Sciences, [8]Department of Human Genetics, Radboud University Nijmegen Medical Centre, 6500 HB Nijmegen, The Netherlands; [9]Department of Biology, University of Miami, Miami, FL 33146, USA; [10]Eaton-Peabody Laboratory, Department of Otology and Laryngology, Massachusetts Eye and Ear Infirmary, Harvard Medical School, Boston, MA 02114, USA; [11]Department of Otology & Skull Base Surgery, Affiliated Eye and ENT Hospital of Fudan University, 83 Fenyang Road, Shanghai, 200031 China; [12]Hearing and Balance Disorders Diagnosis and Rehabilitation Center, Ataturk Research and Training Hospital, 06800 Ankara, Turkey; [13]Department of Life Sciences, Bethlehem University, Bethlehem, Palestine; [14]Department of Otolaryngology and Head-neck Surgery, The Second Xiangya Hospital of Central South University, Changsha 410011, China
[15]These authors contributed equally to this study
*Correspondence: mtekin@med.miami.edu
http://dx.doi.org/10.1016/j.ajhg.2012.09.011.

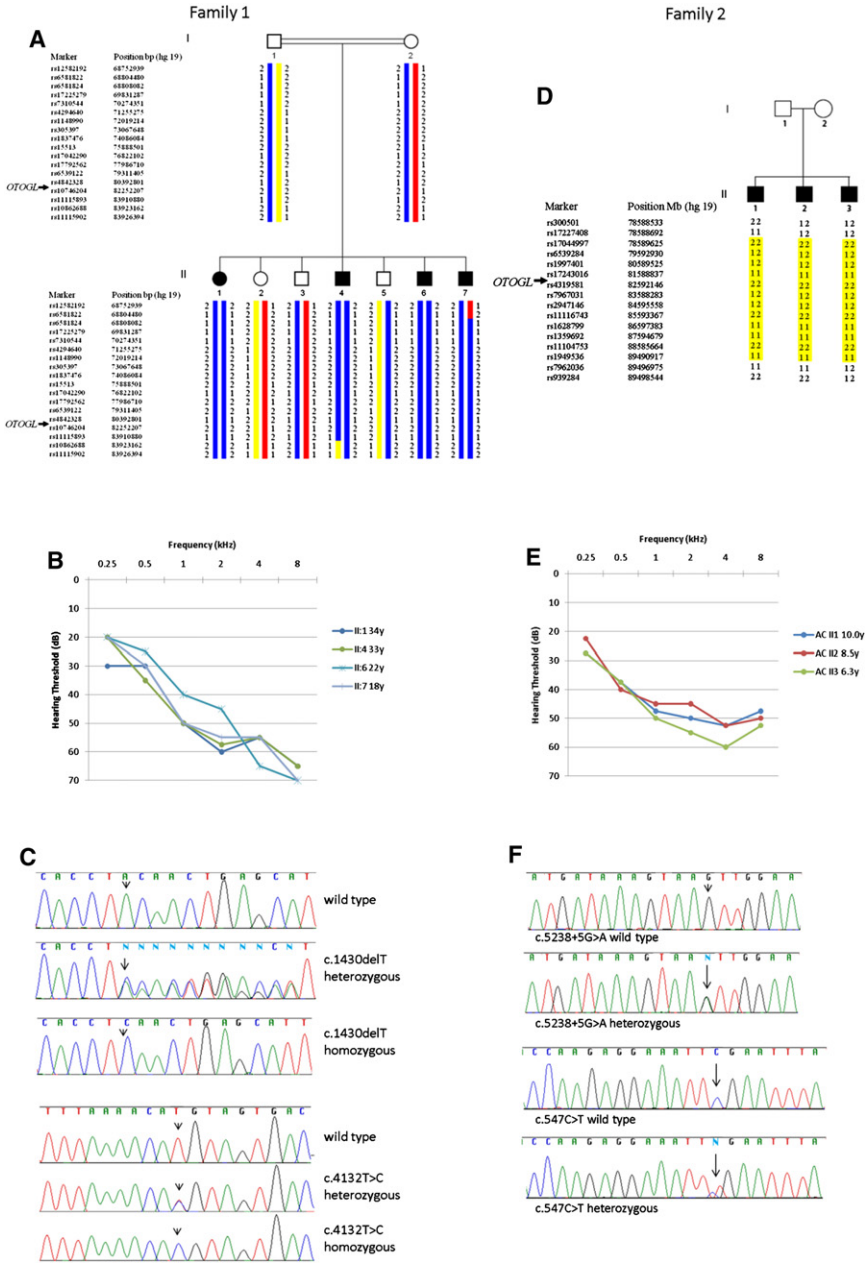

Figure 1. Studied Families, Audiograms, and *OTOGL* Mutations

(A) Family 1 and the longest autozygous region on chromosome 12. Parents are first cousins.

(B) Audiograms show moderate sensorineural hearing loss in family 1.

(C) Electropherograms showing identified mutations in *OTOGL* in family 1.

(D) Pedigree and SNP genotypes in family 2.

(E) Audiograms of affected subjects in family 2 show moderate hearing loss.

(F) Electropherograms of the *OTOGL* mutations identified in family 2.

6 deg/s. Clinical evaluation of all affected individuals by a geneticist and an ENT surgeon included a thorough physical examination and otoscopy. A high resolution CT scan of the temporal bone was obtained in one affected person in each family. The studies presented here were performed in two families: family 1, a consanguineous Turkish family with four children (Figure 1A) and family 2, a nonconsanguineous Dutch family with three children having sensorineural hearing loss (Figure 1D). DNA was extracted from blood via standard methods. One affected individual from each family was prescreened and found not to have common causes of nonsyndromic deafness including mutations in *GJB2* (MIM 121011) and for the m.1555A>G mutation in *MTRNR1* (MIM 561000).

Autozygosity Mapping

Genome-wide SNP genotyping was performed via Affymetrix 6.0 and Illumina Human Omni Express 700K arrays in families 1 and 2, respectively. Autozygosity mapping was performed as reported previously.[6,7] The cosegregation of the genotypes for each previously reported deafness gene was visually evaluated. Multipoint linkage analysis of an autozygous segment was conducted with GeneHunter,[8] assuming a fully penetrant autosomal recessive phenotype with population frequency for the hearing loss allele of 0.0001. SNPs spanning the autozygous region were chosen for linkage analysis based on tagging and heterozygosity in the parents. Copy number variants (CNVs) were assessed by determining the relative loss or gain of fluorescent signal intensity from SNP or CNV probes on the array as previously described.[6]

Whole Exome and Sanger Sequencing

The Agilent SureSelect Human All Exon 50 MB kit was used with an Illumina HiSeq 2000 instrument. Adaptor sequences for the Illumina HiSeq2000 were ligated and the enriched DNA samples were subjected to standard sample preparation for the HiSeq2000 instrument (Illumina). Paired-end reads of 100 bases length were produced. The Illumina CASAVA v1.8 pipeline was used to produce 99 bp sequence reads. BWA[9] was used to align sequence reads to the human reference genome (hg19) and variants were called using the GATK software package.[10] All variants were submitted to SeattleSeq135 for further characterization.

All 58 exons and exon-intron boundaries of *OTOGL* (NM_173591.3) were screened via Sanger-sequencing (detailed in Table S1 available online). To screen additional families for linkage to the *OTOGL* locus, eight SNPs within the gene were chosen, and custom TaqMan probes were developed and assayed according to the manufacturer's protocol. Data were analyzed via SDS 2.3 (Applied Biosystems) software.

Minigene Construction and Splicing Assay

For prediction of the effect of the c.5238+5G>A transition on splicing efficiency, the following software tools were used: NetGene,[11] BDGP Splice prediction site,[12] and Human Splice Finder (Alamut; Interactive Biosoftware).

The splicing assay for the c.5238+5G>A mutation was performed using the pCIneo vector described by Gamundi et al. containing exons 3–5 of *RHO*,[13] which was adapted for the Gateway cloning system by replacing exon 4 and flanking sequences by a Gateway cassette using the EcoNI and PflMI sites of the vector. A fragment containing exon 43 and 225 and 126 bp respectively of 5′and 3′ flanking sequences of *OTOGL* was amplified from genomic DNA of one of the parents of family 2 and clones for the wild-type (WT) and the mutant alleles were selected after sequencing. Primers used for amplification of the fragment are provided in Table S2. Transfection of HEK293T cells with the plasmids, isolation of RNA, and RT-PCR were performed as described.[14] The *RHO* and *OTOGL* exons were amplified from the complimentary DNA (cDNA) with forward primer 5′- cggaggt caacaacgagtct-3′ and reverse primer 5′-aggtgtaggggatgggagac-3′, which are located in *RHO* exon 3 and exon 5, respectively. The assay was performed in triplo in two independent experiments. The RT-PCR fragments were sequenced to verify normal splicing and exon skipping.

OTOGL Expression Profile by Quantitative PCR in Humans

RNA derived from various adult tissues as well as from fetal liver was purchased from Clontech. In addition, RNA was isolated from fetal inner ear, heart, skeletal muscle, and lung as described previously.[15] cDNA was synthesized as previously described[15] and purified with NucleoSpin Extract II columns (Macherey-Nagel) in accordance with the manufacturer's protocol. For PCR, specific primers (Table S2) were designed with Primer3Plus and reference sequence NM_173591.3. Amplifications were performed with the Applied Biosystem Fast 7900 System in accordance with the manufacturer's protocol. The human beta glucuronidase gene (*GUSB*; MIM 611499) was employed as an internal reference. PCR reaction mixtures were prepared with the Power SYBR® Green Master Mix (Applied Biosystems) in accordance with the manufacturer's protocol. Temperatures and reaction times for PCR were as follows: 10 min at 95°C, followed by 40 cycles of 15 s at 95°C and 30 s at 60°C. All reactions were performed in duplicate. Relative gene expression levels were determined with the delta delta Ct method as described previously.[16]

Otogl Expression by Semiquantitative RT-PCR in Mice

Otogl transcript levels in different developmental stages of mouse inner ear were evaluated by semiquantitative RT-PCR. All the procedures were approved by the Institutional Animal Care and Use Committee of the Massachusetts Eye and Ear Infirmary. Mouse cochleae were dissected from CD1 mice at different stages. RNA extractions were performed using Trizol reagent (Life Technologies). Reverse transcriptase reactions were performed using SuperScript II (Life Technologies), and PCR reactions using Taq polymerase (Life Technologies). The PCR primers are given in Table S2. PCR conditions were: 94°C, 2 min; 94°C, 30 s; 62°C, 1 min; 72°C, 1 min 30 s for 40 cycles; 72°C, 10 min. Gene expression was normalized to *GAPDH* expression.

Rodent Immunohistochemistry and In Situ Hybridization

CD1 mouse inner ear tissues from timed pregnancy were collected following an established procedure. The procedure in the use of animals and tissue preparation were approved by the Institutional Animal Care and Use Committee of the Massachusetts Eye and Ear Infirmary and of the Radboud University Nijmegen. Standard immunohistochemical procedures were used for the labeling of cryosectioned mouse cochlear slides, with the antibodies against the following antigens: otogelin-like (OTOGL) (1:150, Atlas Antibodies, HPA040364), SOX2 (1:200, Santa Cruz, sc-17320), MYO7A (1:1,000, Developmental Studies Hybridoma Bank, MYO7A 138-1). The nuclei were labeled with DAPI (1X, Molecular Probe).

For the preadsorption control experiment, the OTOGL antibody was incubated with 10-fold excess (relative to antibody concentration) of OTOGL antigen (Atlas Antibodies, HPA040364, dissolved in 1M urea and 1× PBS) at room temperature for 2 hr. The mixture was spun at 16,000 g for 20′, and the supernatant was used for immunofluorescence. The MYO7A antibody was also mixed with OTOGL antigen and antibody on the same condition and the MYO7A staining was not different from the pattern using the nontreated MYO7A antibody. The image acquisition conditions were identical for all immunolabeling results.

Temporal bones of P10, P20, and P30 Wistar rats were fixed in 2% buffered paraformaldehyde, before dissection of the cochlea and vestibular structures. For these cryosections, the OTOGL antibody was 1:50 diluted and Alexa Fluor 568 labeled phalloidin (1:400; Life Technologies) was added for actin staining. The nuclei were labeled with DAPI (1X, Molecular Probe) and for controls, the primary antibody was omitted. Sections were examined with a fluorescence microscope. In addition, 2% paraformaldehyde fixed whole mount organs of Corti of P12 rats were incubated with anti-otogl (1:50), phalloidin (1:400), and DAPI (1:8,000) as previously described[17] and analyzed with a confocal microscope.

For in situ hybridization, the same sample preparation for mouse inner ear tissue was used as in immunohistochemistry. The protocol used was identical to the one described previously.[18]

Zebrafish *otogl* Identification, Cloning, In Situ Hybridization, and Immunohistochemistry

Zebrafish (*Danio rerio*) were raised and handled following standard techniques[19] approved by the Institutional Animal Care and Use Committee of the University of Miami. Embryos from WT AB stock were used for gene cloning and enhancer trap transgenic line SqET4[20] expressing GFP in hair cells for expression analysis and physiology. We identified the zebrafish homolog of the human *OTOGL* by sequence similarity and synteny analysis. The human OTOGL protein sequence NP_775862.3 was used to query the zebrafish genome version 9 by BLAT using VEGA Genome Browser (release 46), the manually curated zebrafish genomic database. Two high-scoring genomic loci were recovered, *dkeyp-27b10.2*, a predicted *otogl* gene (BX321877.7) on chromosome 18 and (BX842701.1-201) on chromosome 7 that encodes zebrafish *otog*. Separately, linkage analysis of the zebrafish genes to *ptprq*, a deafness gene that in humans is closely linked to *OTOGL*,[7,21] showed that only *dkeyp-27b10.2* is closely associated to the zebrafish *ptprq*. Based on sequence and synteny evidence, we established the zebrafish gene on chromosome 7 as the ortholog of human *OTOG* on chromosome 11 and *dkeyp-27b10.2* on chromosome 18 as the ortholog of human *OTOGL* on chromosome 12. The zebrafish nomenclature committee reviewed and approved these name designations, assigning the Zebrafish Information Network (ZFIN) number ZDB-GENE-120228-1 to *otogelin* (*otog*) and ZDB-GENE-050419-93 to *otogl*.

An 800 base pair region of zebrafish *otogl* near the center of the gene that was devoid of repetitive protein domains was cloned

using an RT-PCR strategy. Nested primers were designed using the zebrafish genome assembly version 9. cDNA from 48 hpf embryos was PCR amplified with Taq polymerase (Promega) and primer set 5out-otogl, TGGAGGAAGGAGTCTGCT and 3out-otogl, CACGGTCACAGGTGCATT. A second round of amplification used inner primers 5in-otogl, GAGTCTGCTGTCCCAAGA and 3in-otogl, CAACCGCAGTCTCCATAC. The PCR cycling parameters used for both reactions was as follows: 94°C, 2 min, 1 time; 94°C, 30 s, 60°C, 1 min, 72°C, 2 min, 35 times; 72°C, 10 min, 4°C, hold, 1 time. PCR product was gel purified, and ligated to pGEM-T Easy (Promega) using manufacturer's instructions. Eight clones were sequenced to verify identity of inserts. One plasmid containing the correct insert was linearized and in vitro transcribed to generate DIG-labeled RNA to use as a probe. Whole-mount in situ hybridization was carried out as previously described,[22] with the following modification: prior to developing the chromogenic reaction with Fast Red substrate (Roche), embryos were immunostained to detect GFP expression in ear hair cells.

Immunodetection of GFP and acetylated-tubulin in zebrafish embryos was done following a previously described protocol.[23] Anti-GFP (Anaspec) and anti-acetylated tubulin (Santa Cruz Biotechnology) were used as primary antibodies and an anti-rabbit Alexa488-conjugated antibody as a secondary antibody (Life Technologies). Actin was detected using Alexa568-conjugated phalloidin (Life Technologies). Immunostaining and in situ hybridization were performed via standard methods.[23]

Zebrafish *otogl* Morpholino Knockdown

To generate zebrafish larvae lacking *otogl* function, we first identified the gene's intron/exon junctions by comparing Otogl protein sequence XP_683212 to the *otogl* genomic region of VEGA. We designed two splice-blocking morpholinos against exon/intron junctions 36 and 37 found at the 3′ half of the gene because the gene's 5′ end is poorly annotated. Missplicing events at these locations were predicted to generate truncated proteins lacking the last von Willebrand Factor (vWF)/cytokine rich paired domains and C-terminal cysteine knot domain. The two splice-blocking morpholinos (GeneTools, LLC) are MO1 GATGCACACACACACT GACCGCAGA against exon/intron junction 36 and MO2 CATCCTGAGGAAAGGAGGGTAACAC against exon/intron junctions 37. The efficacy of *otogl* knockdown by each morpholino was assessed by RT-PCR analysis of morpholino-induced intron retention. Total RNA was extracted from 3-day-old embryos using Trizol (Life Technologies) and treated with Turbo DNase (Ambion). Purified 500 ng RNA was reverse transcribed to cDNA using an anchored oligodT primer and Superscript III (Life Technologies). cDNA (1 μl) was then used as template for a PCR reaction with diagnostic primers TACCACAGCACTGGCATCAT and TTCCTCCAGCTGAAGCAGAT that span the exon/intron junctions targeted by the morpholinos. Primers against an unrelated gene, the glycine receptor β subunit (*glrbb*) serves as a loading control. Morpholinos were titrated to determine the lowest dose that induced missplicing events. Physiology and molecular biology were carried out on embryos injected with 2–5 nL of 0.25 mM *otogl*MO1 or *otogl*MO2. For phenotypic assessment, *otogl* MO-injected larvae were compared to stage-matched larvae injected with the same concentration of a standard control morpholino CCTCTTACCTCAGTTACAATTTATA (GeneTools, LLC). Both *otogl* morpholinos produced similar phenotypes that include severe cardiac edema and, at higher doses, curvature to the body axis.

Microphonic Potential Recording in Zebrafish

The microphonic potential recording from larval zebrafish was modified from previously described protocols.[24,25] Morpholino-injected zebrafish at 2 or 3 dpf were anaesthetized in 0.01% buffered MS-222 solution and embedded dorsal up in 1.8% agarose with 0.01% buffered MS-222 in a low profile 35 mm MatTek dish. The MatTek dish was then placed in a QE-1 platform (Warner Instruments, Hamden, CT) that was temperature controlled at about 28.5°C on a Gibraltar stage of Zeiss Axioskop 2 FS plus microscope. The Zeiss microscope setup rested on an antivibration table and enclosed in a Faraday cage (Technical Manufacturing, Peabody, MA).

A stimulus probe with the tip size of 20 μm in diameter was made from a glass capillary (OD = 1.50 mm, ID = 0.84 mm, World Precision Instruments, Sarasota, FL) using a micropipette puller (P97, Sutter Instrument Co., Novato, CA) and a microforge (MF-900, Narishige International USA, East Meadow, NY). The stimulus probe was driven by a piezoelectric actuator and calibrated using a high-speed camera. The probe tip was placed against the posterior edge of the inner ear (pointing to the saccular otolith) and provided linear oscillatory motion at 200 Hz along an axis parallel to the longitudinal axis of fish body.

The recording electrodes were made from glass capillaries (OD = 1.5, ID = 1.12 mm, WPI), filled with standard fish saline solution (pH = 7.2) and then sharpened with a Sutter BV-10-E micropipette beveler until the electrode resistance dropped to about 6 MΩ. The recording electrode tip was advanced to penetrate the wall of the inner ear of larval zebrafish using a Narishige MHW-3 three-dimensional hydraulic micromanipulator. Microphonic responses were amplified 1,000×, band-pass filtered between 0.1 and 3000 Hz, averaged up to 200 times, and recorded at a sampling rate of 25 kHz. The amplitude of microphonic responses (RMS) was measured at twice the stimulus frequency in FFT plots. Student's t test was performed to determine the significance of differences in microphonic amplitude between *otogl* morphants and larvae injected with a control morpholino.

Results

OTOGL Mutations Cause Moderate Sensorineural Hearing Loss in Humans

In family 1, all four affected individuals had symmetric moderate sensorineural hearing loss. Available audiograms did not show progression (Figure 1B; Figure S1). Clinical examinations did not reveal additional findings. CT scan of the temporal bone of one affected family member was normal as well. Detailed vestibular analyses were performed in one individual, II:7, who complained about one episode of dizziness lasting for 3 months at age 17. He described it as a blurry vision caused by turning his head abruptly to the left and lasting for only a few seconds. There were no other symptoms such as vertigo. Vestibular tests revealed vestibular hypofunction on the left side via caloric tests. All positional tests produced persistent up-left nontorsional nystagmus with the average of 7 deg/s without vertigo sensation.

Only one autozygous genomic region larger than 1 Mb was shared by all four affected members of family 1. The length of this autozygous region was 15 Mb on

Table 1. The Number of Variants, SNPs and Indels, Identified by Whole Exome Sequencing of One Individual in Family 1 Compared to the Reference Genome hg19. The Different Filters and Annotation Categories Are Shown

Region	Total Variants	Novel Variants
Whole exome	221,686	77,655
+Homozygous variants	64,180	2,828
+Chr12:68,804,480-83,923,162	407	38
+Missense, nonsense, splice, frameshift	16	2
Sanger confirmed	NA	2 in *OTOGL*

NA, not available.

chromosome 12 (68,804,480–83,923,162 bp) and included the DFNB84 locus (Figure 1A). The autozygous region contains 51 RefSeq genes including *PTPRQ* (MIM 603317), which was recently found to be associated with arNSHL.[7,21] A multipoint LOD score of 3.36 was obtained for this region. Sanger-sequencing of the exons and intron-exon boundaries of *PTPRQ* (NM_001145026.1) in one affected member did not show a mutation. None of the other previously identified deafness genes mapped to an autozygous region suggesting that a previously unrecognized human deafness gene was involved in this family.

We then performed whole exome sequencing in individual II:7, which generated 177,257,596 reads. Using a minimum depth of 4×, 84% of the targeted regions were covered with an average read depth of 100×. The longest autozygous region on chromosome 12 was fully covered by SureSelect Human All Exon 50 Mb kit except for *PTPRQ*, which was Sanger-sequenced in family 1. After multiple filters were employed (Table 1), whole exome data revealed two novel homozygous variants both located in *OTOGL* (hg19): a one base pair deletion at 80,648,835, c.1430 delT (NM_173591.3) predicted to cause a reading frame shift and a premature termination of protein synthesis, p.Val477Glufs*25 (NP_775862.3) and 80,717,580T>C corresponding to c.4132T>C (NM_173591.3) predicted to lead to the substitution of an arginine for a cysteine, p.Cys1378Arg (NP_775862.3). Both variants were confirmed via Sanger sequencing (Figure 1C). They both cosegregated with the phenotype in the family as an autosomal recessive trait and were absent in 373 ethnicity-matched control samples. Neither variant has been found in the NHLBI Exome Sequencing Project (Exome Variant Server), or in dbSNP databases. The p.Cys1378Arg variant affected a highly conserved residue in *OTOGL*. However, because p.Cys1378Arg is located at the C-terminal relative to p.Val477Glufs*25, it is unlikely to contribute to the phenotype. Screening for additional mutations in *OTOGL* via linkage analysis followed by Sanger-sequencing in additional 195 families with severe or profound arNSHL failed to detect a mutation.

Three brothers in family 2 presented moderate and stable hearing loss. Physical examination and otoscopy revealed no abnormalities. Diagnosis of hearing loss was at the neonatal hearing screening for II:3 and can therefore be assumed to be congenital. Subsequently, the older brothers were diagnosed at the ages of 3 (II:1) and 2 (II:2) years. All three boys performed normally in the Unterberger, Romberg, head thrust, and head shake tests, and, in addition, the eye tracking movements, although a delay in gross motor development was reported. A high resolution CT scan in II:3 did not reveal abnormalities. Autozygosity mapping in family 2 did not reveal any significant homozygous regions (>1 Mb) shared by all three affected children. As a next step, the data were analyzed for the presence of shared genotypes (>3 Mb) in the three affected children for the previously described autosomal recessive deafness loci; a shared region of 10.9 Mb on chromosomal region 12q21.2-q21.32 was identified encompassing the DFNB84 locus. Because of the moderate, stable nature of the hearing impairment that was also noted in family 1, we initiated mutation analysis of *OTOGL*. Two variants, which were not present in the NCBI dbSNP134 or 135 database, NHLBI Exome Sequencing Project (Exome Variant Server), nor in the 1000 Genomes Project, were identified; a nonsense mutation c.547C>T (p.Arg183*) and a splice site mutation c.5238+5G>A. All three affected children were compound heterozygous for these mutations; father and mother were heterozygous for p.Arg183* and c.5238+5G>A, respectively. The splice site mutation is predicted to reduce splicing efficiency by ~50% (0.47 versus 0.98 for the WT sequence; BDGP Splice Prediction). Two other prediction tools, NetGene Splice site predictions and Human Splice Finder, do not predict a splice donor site for the sequence with the G to A transition. A minigene assay was performed to test the effect of the mutation on splicing in HEK293T cells, which demonstrated skipping of exon 43 (Figure S2).

Otogelin-like, the predicted product of *Otogl*, was recently identified in mouse by amplification and sequencing of the transcript. The gene was annotated and named because of its structural similarity to otogelin.[21] Otogelin encoded by *Otog* was first discovered as an extracellular glycoprotein specific to the acellular membranes of inner ear.[26] Otogelin shows structural similarities to the epithelial-secreted mucin protein family because it comprises an N-terminal signal peptide, a central threonine/serine/proline-rich (TSP) region flanked by vWF-like cysteine-rich domains, and a C-terminal knot motif domain.[26] Otogelin-like similarly contains an N-terminal signal peptide of 22 amino acids in the N-terminal (predicted by the SignalP software) as well as vWF and knot domains in the mature peptide (Figure 4B). Otogelin and otogelin-like have an amino acid identity of 33.3% (56.0% similarity).

Expression Profile of *OTOGL*

The expression of *OTOGL* relative to *GUSB* standard internal control was studied via quantitative PCR (qPCR) in ten adult and ten fetal-stage human tissues including

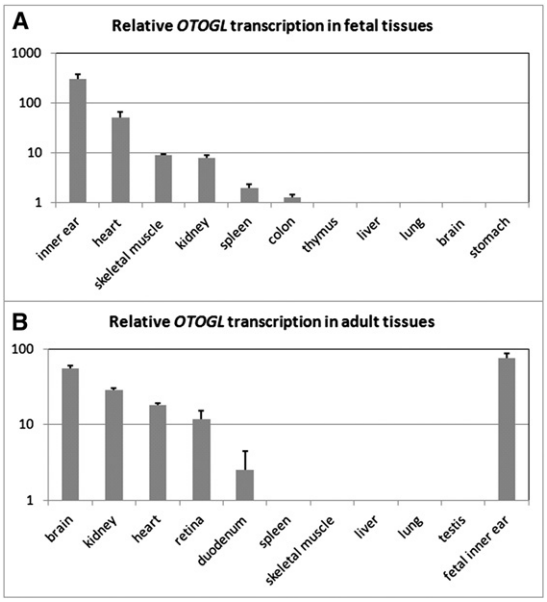

Figure 2. *OTOGL* Expression Profile in Human Tissues
Relative *OTOGL* mRNA levels as determined by qPCR in human fetal (A) and adult (B) tissues. The relative expression values were determined by using the delta delta Ct method. Relative *OTOGL* transcript levels were highest in fetal inner ear.

human fetal inner ear (Figure 2). Because this was performed for adult and fetal tissues in two separate experiments, fetal inner ear was included in both for comparison. In adult tissues, relatively low *OTOGL* transcript levels as compared to fetal inner ear were seen in lung, spleen, and duodenum and relatively moderate levels in heart, kidney, brain, and retina. In three of the adult tissues—skeletal muscle, liver and testis—expression of *OTOGL* was below the detection level. Among the fetal tissues that were tested, the transcript level was highest in the inner ear. However, because these tissues were not derived from fetuses of the same gestational stage, a direct comparison of the transcript levels cannot be made. The inner ear was derived from a fetus at 8 weeks of gestation and all other fetal tissues from fetuses at 20–21 weeks gestation. At the latter stage, *OTOGL* transcript levels were highest in fetal heart. A low relative *OTOGL* transcript level was observed in skeletal muscle, kidney, spleen, and colon. In the fetal liver, lung, brain, and stomach, expression was below the detection level.

Otogelin-like Is Present in Several Cell Types and the Acellular Membranes of the Inner Ear

The localization of OTOGL in the inner ear was studied by immunostaining with an anti-OTOGL antibody in the mouse and rat. Furthermore, we analyzed the transcription of *otogl* by in situ hybridization in the mouse and zebrafish and by semiquantitative RT-PCR in the mouse. Overall OTOGL showed a dynamic expression pattern throughout development, and immunostaining and in situ results were consistent with each other. At E17.5, OTOGL was primarily detected in the spiral prominence and the Claudius cells and weakly in hair cells (Figures 3A and 3B). It was detected in the lumen surface of interdental cells in the proximity of Reissner's membrane (Figure 3A, arrowhead) and in the base of nascent tectorial membrane (Figure 3A, arrow). A similar OTOGL distribution was detected in P0 cochlea (Figure 3C), with additional detection in some supporting cells. In saccule, OTOGL was detected weakly in hair cells and more prominently in the saccular roof (Figure 3E). By P6, OTOGL distribution became more restricted. It was detected mainly in the outer hair cells, Deiters cells, and Claudius cells (Figure 3F). In the tectorial membrane, it was localized to the base (Figure 3F, arrow). In the saccule, elevated level was detected in the saccule roof with little change in the hair cells (Figure 3H). To study the specificity of the antibody staining, we performed preadsorption with a synthesized peptide containing the OTOGL antigen as control. Preadsorption abolished the signals revealed by the OTOGL antibody but did not affect Myo7a (Figure 3G), demonstrating the specificity of the OTOGL antibody.

By semiquantitative RT-PCR, *Otogl* was upregulated up to P13 in the cochlea and downregulated in the adult. In addition to the inner ear, *Otogl* transcript was detected weakly in the cortex, but not in the hippocampus (Figure 3J).

In the rat, OTOGL continued to be present in various inner ear cells, particularly in Hensen's cells in the postnatal period, and was present in the acellular membranes and basilar membrane (Figures S3 and S4).

In zebrafish, *otogl* transcription during the first 5 days of larval development was confined to the otic vesicle (Figure 4A; data not shown). Using fluorescent in situ hybridization, we first detected *otogl* transcripts at 36 hr post fertilization in the developing macula communis (Figure 4A).[22] At later developmental stages *otogl* expression was also detected in the other maculae (Figure 4A and not shown). Within the maculae, two different apical epithelial cell populations were found to express *otogl*, hair and nonhair cells (Figure 4A; data not shown). In older larvae, *otogl* transcription was also seen in many basal epithelial cells directly below hair cells (Figure 4A). Thus, different populations of basal and apical cells associated with the maculae express *otogl*.

Knocking Down *otogl* in Zebrafish Causes Sensorineural Hearing Loss and Anatomical Changes in the Inner Ear

To determine the function of *otogl*, we knocked down the expression of the highly conserved Otogl protein (XP_683212; 73.1% identity over a stretch of 746 amino acids) in zebrafish by injecting splice-junction blocking morpholinos (MOs) into fertilized eggs. Both human and predicted zebrafish Otogl are large proteins, 2,343 and 2,454 aa respectively, consisting of four repeats of paired vWF/C8 (von Willebrand Factor/cysteine rich) domains with a C-terminal cystine knot domain (Figure 4B). Other

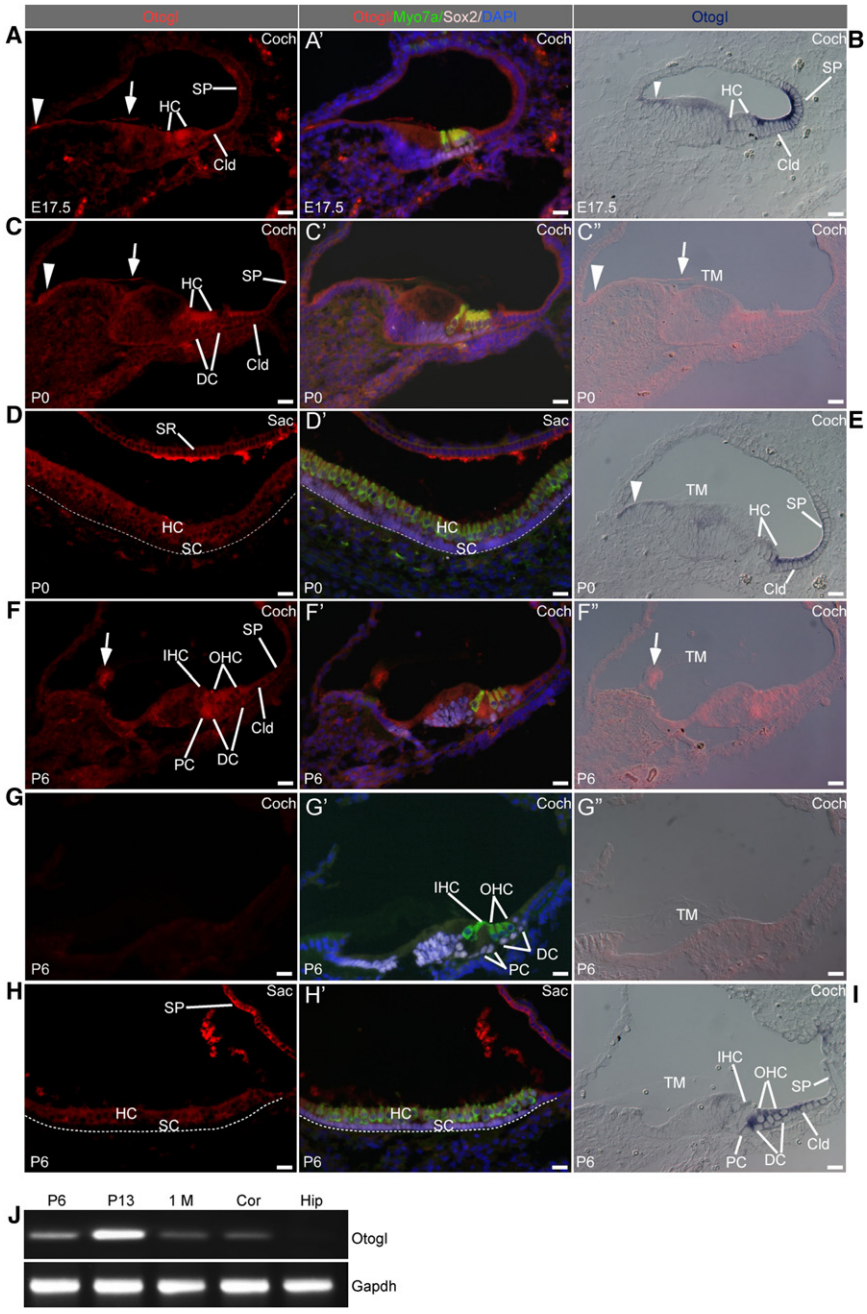

Figure 3. *Otogl* Expression and Distribution in the Mouse Inner Ear

(A and A') In E17.5 cochlea, OTOGL was detected by immunohistochemistry on the lumen surface of interdental cells close to the Reissner's membrane (arrowhead), the base of tectorial membrane (arrow), hair cells (HC), Claudius cells (Cld), and spiral prominence (SP). Figures in the middle column (A'–G') are merged images that include the first column.

(B) By in situ hybridization, *Otogl* mRNA was detected in the same cell types as shown by immunostaining, with the difference that immunolabeling also detected staining on the surface (A, arrowhead and arrow). Scale bars represent 20 μm.

(C) In P0 cochlea, a similar OTOGL distribution pattern was detected by immunostaining, with clear presence in the Deiters cells (DC). The figure on the third column (C″) is a merged picture from Otogl labeling with a differential interference contrast (DIC) image, to show the tectorial membrane (TM).

(D) In P0 saccule, OTOGL was weakly detected in hair cells, but prominently detected in the saccular roof (SR). The strong labeling on the surface of the SR was likely the otolithic membrane. The dashed line represents the base of the basilar membrane.

(E) In situ hybridization showed *Otogl* expression in the cochlea that was consistent with immunolabeling results.

(F) In P6 cochlea, OTOGL distribution was restricted to outer hair cells (OHC), Pillar cells, Deiters cells, and Claudius cells. In the tectorial membrane, it was limited to the base (arrow).

(G) Preadsorption with a synthetic OTOGL antigen eliminated the signals reveled by the OTOGL antibody including TM staining.

(H) In the P6 saccule, OTOGL distribution was similar to that at P0, however with a higher level in the saccular roof.

(I) The level of *Otogl* mRNA was enhanced in the OHC, Deiters, and Pillar cells.

(J) Semiquantitative RT-PCR of whole cochlea showed that *Otogl* transcripts were most abundant at P13 and decreased in toward young adulthood. *Otogl* was also detected in the cortex (Cor) but not in the hippocampus (Hip). *Gapdh* transcript levels were used as a control.

proteins with this domain structure are mucin and otogelin.[26] We designed two splice-junction blocking morpholinos against exon/intron 36 and 37 of the zebrafish gene that result in protein truncations (Figures 4B and 4C). Both *otogl*MO1 and *otogl*MO2 morphants significantly knocked down the expression of *otogl* at day 2 (Figure 4C). *otogl*MO2 morphants were used for inner ear morphological analysis and physiological recordings because MO1 caused severe cardiac edema. MO2 morphant phenotypes were characterized by mild cardiac edema, slight reduction in larvae length (t test, $p = 0.007$), failure to escape in response to vibration stimuli, a smaller inner ear ($p = 0.002$), and smaller saccular otolith ($p = 0.001$) (Figures 4D and 4E). There was no significant difference in size of utricular otolith between the control and morphants ($p = 0.41$). Furthermore, loss of *otogl* function also caused defects in the development of the tissue pillars that shape the semicircular canals (Figures 4F and 4G). It is unclear if these misshapen semicircular canals impacted vestibular function, as the severe cardiac edema precluded the analysis of circling behaviors at day 5 postfertilization that are characteristic of vestibular deficits.[27] Microphonic

potentials were recorded from controls and *otogl*MO2 morphants in response to oscillatory stimulation at 200 Hz and ± 3 μm in displacement. The microphonic waveforms recorded had a characteristic feature of doubling of the stimulus frequency (Figure 4H). The average amplitude of microphonic responses that were measured at 400 Hz in FFT plots ranged from 14 ± 8 μV (N = 11) for control morphlino-injected larvae and 4 ± 5 μV (n = 12) for *otogl* morphants (Figure 4I). Microphonic responses of *otogl* morphants are significantly smaller than those of controls ($p = 0.0008$).

Discussion

We present mutations in *OTOGL* as a cause of nonsyndromic deafness at the DFNB84 locus where mutations in *PTPRQ* were previously discovered.[7,21] We focused on this genomic region because statistically significant linkage was obtained in a genome scan and we found a truncating mutation in *OTOGL* via whole exome sequencing. A second multiplex family was independently identified with two compound heterozygous mutations, which provided further genetic support for the causative role of *OTOGL* mutations in hearing loss. We subsequently showed that *OTOGL* is preferentially expressed in the inner ear in various species and that knocking down *otogl* leads to sensorineural hearing loss in zebrafish. We thus present mutations in *OTOGL* as a cause of hereditary deafness. The clinical phenotype is quite similar in the two families with *OTOGL* mutations and is characterized by a stable, moderate sensorineural hearing loss. One affected person tested demonstrated vestibular abnormalities, indicating that mutations in *OTOGL* may cause vestibular dysfunction.

Sensory epithelia of the vertebrate inner ear consist of highly organized arrays of sensory hair cells and supporting cells. The acellular membranes of the inner ear form intimate contact with the stereocilia bundles of the hair cells. Each neuroepithelium of the inner ear is covered by an acellular gelatinous membrane: a voluminous gelatinous substance forming a dome-shaped cupula sits on top of each crista in the ampullae of the semicircular canals. In the utricle and saccule, an otoconial membrane loaded with crystal-like structures, the otoconia, covers the surface of the macula. In the cochlea, a tectorial membrane overlies the auditory epithelia.[28] These extracellular matrices generally serve to either transmit the primary stimulus to the stereocilia bundle or act as structures against which the stereocilia bundles can react. They also serve to load the bundles and change their resonance frequency.[29] Acellular membranes of the inner ear contain various collagens and noncollagenous proteins that include α-tectorin (TECTA), β-tectorin (TECTB), and otogelin (OTOG).[28] In this study, we show that otogelin-like is an additional component of the inner ear acellular membranes that plays important functional roles in hearing.

In the mammalian inner ear, the cupula, the otoconial membrane, and the tectorial membrane exhibit a progressive increase in molecular and structural complexity, with the cupula appearing the least complex and the tectorial membrane the most complex.[28] This increase of complexity may reflect changes that occurred in the acellular membranes of the inner ear as a mammalian hearing organ arose during evolution from a simple equilibrium receptor.[28] Otogelin was shown to be present in all three membranes, suggesting a fundamental and ancient role for this protein.[28] Our study shows that the expression pattern of otogelin-like is similar to that of otogelin by its presence in all three acellular membranes of the inner ear and in all four species analyzed; zebrafish, mouse, rat, and human.

Our data show that *Otogl* is mainly expressed in Claudius cells, Hensen's cells, and outer hair cells with a transcription level that is high in embryonic, lower in neonatal, and much lower in adult stages. The protein product, however, is also prominently present in the acellular structures. High levels of transcription of *Otogl* in early and downregulation of the gene in later development strongly suggests that otogelin-like, similarly to other acellular structure components such as otogelin, is normally involved in the production of the structure, which may require relatively low of gene activity for the maintenance on the continuous basis.[30]

Although a human phenotype of *OTOG* mutations has not been reported yet, targeted disruption of *Otog* resulted in deafness and severe imbalance in mice.[31] Histological analysis of these mutants demonstrated that in the vestibule, otogelin was required for the anchoring of the otoconial membranes and cupulae to the neuroepithelia. In the cochlea, ultrastructural analysis of the tectorial membrane indicated that otogelin was involved in the organization of its fibrillar network. Thus, otogelin is likely to have a role in the resistance of this membrane to sound stimulation.[31] Because of structural and expressional similarities, it is possible that otogelin-like plays a similar role in the inner ear. The clinical phenotype in humans with a stable hearing loss and vestibular findings further supports this possibility. On the other hand, the functions of otogelin-like and otogelin are highly likely to be at least partially noncompensatory, as mutations in each of the corresponding genes can cause hearing loss.

Supplemental Data

Supplemental Data includes four figures and two tables and can be found with this article online at http://www.cell.com/AJHG/.

Acknowledgments

We want to acknowledge the families for their participation in the study. This work was supported by National Institutes of Health grants R01DC009645 to M.T., R01 DC006908 to Z.-Y.C, R21 DC009879 to Z. L., RO1DC05575 to X.-Z.L., the Fredrick and

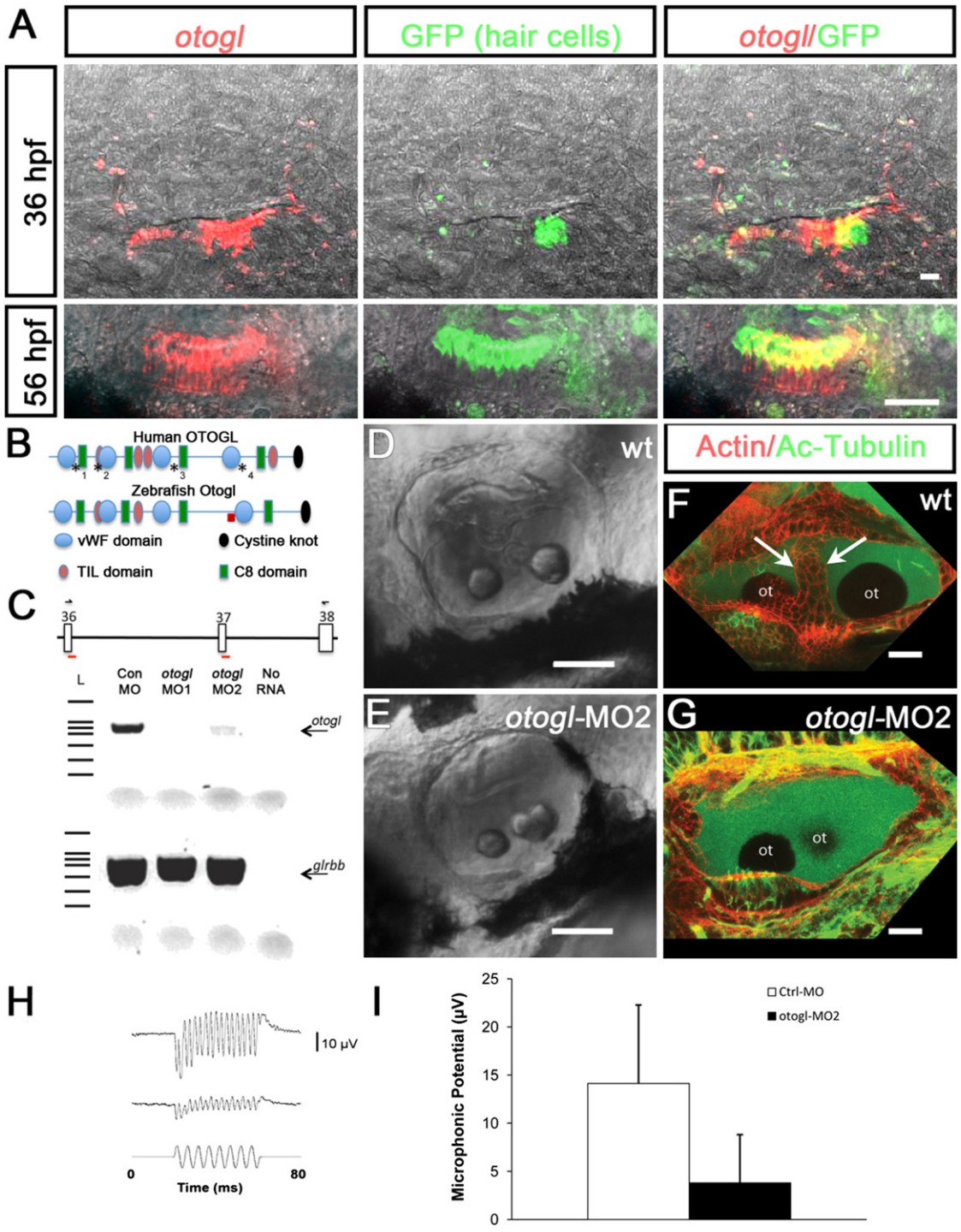

Figure 4. ***otogl*** **Expression and Loss of Function Analysis in Zebrafish**

(A) Expression of *otogl* (red, in situ hybridization) in ear epithelial cells and its relation to hair cell development (green, GPF immunostaining). Sagittal confocal images of developing otocysts showing, at 36 hr postfertilization (hpf), initial *otogl* expression in the forming macula communis, and, at 56 hpf, in the macula of the utricle. Throughout larval stages, most hair cells in all maculae express *otogl*, but some *otogl*-negative hair cells can also be seen (data not shown). Many basal ear epithelial cells directly below hair cells also express *otogl*. Scale bars represent 25 μm; embryos are mounted anterior to the left.

(B) Diagrams comparing the structural organization of human OTOGL and zebrafish Otogl four vWF/C8 domains (von Willebrand Factor [blue ovals]/cysteine rich [green rectangles] domains), four Trypsin Inhibitor-like domains (TIL domains, pink ovals) and one C-terminal cystine knot domain (black oval). These diagrams are adapted from the output of SMART. The location of human mutations (1.p.Arg183*; 2.p.Val477Glufs*25; 3.p.Cys1378Arg; 4.c.5238+5G>A) are indicated by asterisks and the location of the zebrafish missplicing site targeted by the morpholinos is indicated by a red box.

(C) Diagram of zebrafish *otogl* exons 36, 37, and 38 showing the targeting site of MO1 at exon/intron junction 36 and the targeting site of MO2 at intron/exon-junction 37 (red bars). Position of diagnostic PCR primers is indicated in exons 36 and 37 (back arrows). Below the

Ines Yeatts Inner Ear Hair Cell Regeneration Fellowship to M.H. and N.L., the Heinsius Houbolt Foundation to H.K., the Oticon Foundation (09-3742) to H.K., ZonMW to H.K. (40-00812-98-09047) and R.J.E.P. (90700388), and the RNID (GR36) to H.K. N.L. was supported by a grant from the China Scholarship Council, P.R. China. X.Z.L. was supported by Hurong Scholar Award in Hunan, China. Z.L. and J.D. were supported by the University of Miami Provost Research Award and College of Arts. Z.L. was supported by Sciences Gabelli Fellowship. I.S. was supported by National Science Foundation grant IOS-0920449 and by the University of Miami Provost Research Award. We are grateful to Atlas Antibodies for providing the OTOGL immunogenic peptide.

Received: February 28, 2012
Revised: August 1, 2012
Accepted: September 19, 2012
Published online: November 1, 2012

Web Resources

The URLs for data presented herein are as follows:

Ensembl, http://www.ensembl.org
Exome Variant Server, NHLBI Exome Sequencing Project (ESP), http://evs.gs.washington.edu/EVS/
ExonPrimer, http://ihg2.helmholtz-muenchen.de/ihg/ExonPrimer.html
Hereditary hearing loss homepage, http://hereditaryhearingloss.org/
Online Mendelian Inheritance in Man, http://www.omim.org
Polyphen-2, http://genetics.bwh.harvard.edu/pph2/
Primer3plus, http://www.bioinformatics.nl/cgi-bin/primer3plus/primer3plus.cgi
SIFT, http://sift.jcvi.org/
SignalP, http://www.cbs.dtu.dk/services/SignalP-4.0/
Simple Modular Architectural Research Tool (SMART), http://smart.embl-heidelberg.de/.
The 1000 Genomes Project, http://www.1000genomes.org/
The SeattleSeq annotation, http://snp.gs.washington.edu/SeattleSeqAnnotation
Zebrafish VEGA genome browser, http://vega.sanger.ac.uk/Danio_rerio/Info/Index

References

1. Lenz, D.R., and Avraham, K.B. (2011). Hereditary hearing loss: from human mutation to mechanism. Hear. Res. *281*, 3–10.
2. Morton, C.C., and Nance, W.E. (2006). Newborn hearing screening—a silent revolution. N. Engl. J. Med. *354*, 2151–2164.
3. Duman, D., Sirmaci, A., Cengiz, F.B., Ozdag, H., and Tekin, M. (2011). Screening of 38 genes identifies mutations in 62% of families with nonsyndromic deafness in Turkey. Genet Test Mol Biomarkers *15*, 29–33.
4. Francey, L.J., Conlin, L.K., Kadesch, H.E., Clark, D., Berrodin, D., Sun, Y., Glessner, J., Hakonarson, H., Jalas, C., Landau, C., et al. (2012). Genome-wide SNP genotyping identifies the Stereocilin (STRC) gene as a major contributor to pediatric bilateral sensorineural hearing impairment. Am. J. Med. Genet. A. *158A*, 298–308.
5. Marlin, S., Feldmann, D., Blons, H., Loundon, N., Rouillon, I., Albert, S., Chauvin, P., Garabédian, E.N., Couderc, R., Odent, S., et al. (2005). GJB2 and GJB6 mutations: genotypic and phenotypic correlations in a large cohort of hearing-impaired patients. Arch. Otolaryngol. Head Neck Surg. *131*, 481–487.
6. Sirmaci, A., Erbek, S., Price, J., Huang, M., Duman, D., Cengiz, F.B., Bademci, G., Tokgöz-Yilmaz, S., Hişmi, B., Ozdağ, H., et al. (2010). A truncating mutation in SERPINB6 is associated with autosomal-recessive nonsyndromic sensorineural hearing loss. Am. J. Hum. Genet. *86*, 797–804.
7. Schraders, M., Oostrik, J., Huygen, P.L., Strom, T.M., van Wijk, E., Kunst, H.P., Hoefsloot, L.H., Cremers, C.W., Admiraal, R.J., and Kremer, H. (2010). Mutations in PTPRQ are a cause of autosomal-recessive nonsyndromic hearing impairment DFNB84 and associated with vestibular dysfunction. Am. J. Hum. Genet. *86*, 604–610.
8. Kruglyak, L., Daly, M.J., Reeve-Daly, M.P., and Lander, E.S. (1996). Parametric and nonparametric linkage analysis: a unified multipoint approach. Am. J. Hum. Genet. *58*, 1347–1363.
9. Li, H., and Durbin, R. (2009). Fast and accurate short read alignment with Burrows-Wheeler transform. Bioinformatics *25*, 1754–1760.
10. McKenna, A., Hanna, M., Banks, E., Sivachenko, A., Cibulskis, K., Kernytsky, A., Garimella, K., Altshuler, D., Gabriel, S., Daly, M., and DePristo, M.A. (2010). The Genome Analysis Toolkit: a MapReduce framework for analyzing next-generation DNA sequencing data. Genome Res. *20*, 1297–1303.
11. Bohr, H., Bohr, J., Brunak, S., Cotterill, R.M., Lautrup, B., Nørskov, L., Olsen, O.H., and Petersen, S.B. (1988). Protein secondary structure and homology by neural networks. The alpha-helices in rhodopsin. FEBS Lett. *241*, 223–228.
12. Reese, M.G., Eeckman, F.H., Kulp, D., and Haussler, D. (1997). Improved splice site detection in Genie. J. Comput. Biol. *4*, 311–323.

diagram, a DNA gel demonstrates efficacy and specificity of *otogl* morpholinos. The gel shows RT-PCR products generated from 500 ng RNA harvested from 56 hpf embryos injected at the one-cell stage either with control morpholino (Con MO), *otogl*MO1, or *otogl*MO2. Two primer sets amplify either *otogl* (top row) or *glrbb* (bottom row; internal control) from cDNA synthesized using anchored oligodT primers. L indicates the DNA ladder. A sample without RNA was used as a negative control (no RNA). The faint bands at the bottom of the gel are unincorporated primers.
(D and E) Loss of *otogl* function by *otogl*MO2 causes inner ear and saccular otolith malformations (E, n = 3) compared to stage matched, 56 hpf, WT embryos (D, n = 5). Bar is 50 μm. Embryos mounted anterior to the left.
(F and G) Confocal microscope images of 56 hpf control (F, n = 5) and *otogl*MO2 (G, n = 3) embryos show that inner ear malformations are due to defects in the development of the tissue pillars that form the semicircular canals (arrows in F). Scale bars are 20 μm. Embryos were mounted anterior to the left.
(H) Microphonic responses from the inner ear of control (top trace) and *otogl*MO2 morphants (middle trace) at 56 hpf. The bottom trace is the stimulus mwaveform at 200 Hz and ± 3 μm displacement.
(I) Histograms showing the means ± SD of microphonic responses that were averaged 200 times for control morphants and *otogl*MO2 morphants.

13. Gamundi, M.J., Hernan, I., Muntanyola, M., Maseras, M., López-Romero, P., Alvarez, R., Dopazo, A., Borrego, S., and Carballo, M. (2008). Transcriptional expression of cis-acting and trans-acting splicing mutations cause autosomal dominant retinitis pigmentosa. Hum. Mutat. *29*, 869–878.
14. de Heer, A.M., Collin, R.W.J., Huygen, P.L.M., Schraders, M., Oostrik, J., Rouwette, M., Kunst, H.P.M., Kremer, H., and Cremers, C.W. (2011). Progressive sensorineural hearing loss and normal vestibular function in a Dutch DFNB7/11 family with a novel mutation in *TMC1*. Audiol. Neurootol. *16*, 93–105.
15. Luijendijk, M.W., van de Pol, T.J., van Duijnhoven, G., den Hollander, A.I., ten Caat, J., van Limpt, V., Brunner, H.G., Kremer, H., and Cremers, F.P. (2003). Cloning, characterization, and mRNA expression analysis of novel human fetal cochlear cDNAs. Genomics *82*, 480–490.
16. Livak, K.J., and Schmittgen, T.D. (2001). Analysis of relative gene expression data using real-time quantitative PCR and the 2(-Delta Delta C(T)) Method. Methods *25*, 402–408.
17. Stapelbroek, J.M., Peters, T.A., van Beurden, D.H., Curfs, J.H., Joosten, A., Beynon, A.J., van Leeuwen, B.M., van der Velden, L.M., Bull, L., Oude Elferink, R.P., et al. (2009). ATP8B1 is essential for maintaining normal hearing. Proc. Natl. Acad. Sci. USA *106*, 9709–9714.
18. Huang, M., Sage, C., Li, H., Xiang, M., Heller, S., and Chen, Z.Y. (2008). Diverse expression patterns of LIM-homeodomain transcription factors (LIM-HDs) in mammalian inner ear development. Dev. Dyn. *237*, 3305–3312.
19. Westerfield, M. (2000). The Zebrafish Book. A Guide for the Laboratory use of Zebrafish (Danio Rerio) (Eugene, OR: Univ. of Oregon Press).
20. Go, W., Bessarab, D., and Korzh, V. (2010). atp2b1a regulates Ca(2+) export during differentiation and regeneration of mechanosensory hair cells in zebrafish. Cell Calcium *48*, 302–313.
21. Shahin, H., Rahil, M., Abu Rayan, A., Avraham, K.B., King, M.C., Kanaan, M., and Walsh, T. (2010). Nonsense mutation of the stereociliar membrane protein gene PTPRQ in human hearing loss DFNB84. J. Med. Genet. *47*, 643–645.
22. Haddon, C., and Lewis, J. (1996). Early ear development in the embryo of the zebrafish, Danio rerio. J. Comp. Neurol. *365*, 113–128.
23. Skromne, I., Thorsen, D., Hale, M., Prince, V.E., and Ho, R.K. (2007). Repression of the hindbrain developmental program by Cdx factors is required for the specification of the vertebrate spinal cord. Development *134*, 2147–2158.
24. Starr, C.J., Kappler, J.A., Chan, D.K., Kollmar, R., and Hudspeth, A.J. (2004). Mutation of the zebrafish choroideremia gene encoding Rab escort protein 1 devastates hair cells. Proc. Natl. Acad. Sci. USA *101*, 2572–2577.
25. Corey, D.P., García-Añoveros, J., Holt, J.R., Kwan, K.Y., Lin, S.Y., Vollrath, M.A., Amalfitano, A., Cheung, E.L., Derfler, B.H., Duggan, A., et al. (2004). TRPA1 is a candidate for the mechanosensitive transduction channel of vertebrate hair cells. Nature *432*, 723–730.
26. Cohen-Salmon, M., El-Amraoui, A., Leibovici, M., and Petit, C. (1997). Otogelin: a glycoprotein specific to the acellular membranes of the inner ear. Proc. Natl. Acad. Sci. USA *94*, 14450–14455.
27. Moorman, S.J., Cordova, R., and Davies, S.A. (2002). A critical period for functional vestibular development in zebrafish. Dev. Dyn. *223*, 285–291.
28. Goodyear, R.J., and Richardson, G.P. (2002). Extracellular matrices associated with the apical surfaces of sensory epithelia in the inner ear: molecular and structural diversity. J. Neurobiol. *53*, 212–227.
29. Manley, G.A. (2000). Cochlear mechanisms from a phylogenetic viewpoint. Proc. Natl. Acad. Sci. USA *97*, 11736–11743.
30. El-Amraoui, A., Cohen-Salmon, M., Petit, C., and Simmler, M.C. (2001). Spatiotemporal expression of otogelin in the developing and adult mouse inner ear. Hear. Res. *158*, 151–159.
31. Simmler, M.C., Cohen-Salmon, M., El-Amraoui, A., Guillaud, L., Benichou, J.C., Petit, C., and Panthier, J.J. (2000). Targeted disruption of otog results in deafness and severe imbalance. Nat. Genet. *24*, 139–143.